Hydroforming for Small Hollow Protrusion in T- and X-Shaped Joints

Quang Vu Duc
Faculty of Mechanical Engineering, University of Economics - Technology for Industries, No. 456 Minh Khai, Vinh Tuy Ward, Hanoi City, Vietnam
vuquang@uneti.edu.vn (corresponding author)

Received: 22 August 2025 | Revised: 18 September 2025 and 24 September 2025 | Accepted: 27 September 2025

 DOI: https://doi.org/10.48084/etasr.14242

ABSTRACT

Traditional stamping and welding methods for creating small hollow protrusions in joints often lead to uneven deformation, material thinning, residual stress, and thermal stress. These issues compromise the material continuity, reduce the structural stiffness, and weaken the overall strength. This study applies the Tube Hydroforming (THF) process to improve the formation of small hollow protrusions in T- and X-shaped copper joints. Finite Element Method (FEM) simulations were carried out in Abaqus/CAE using a plastic material model and nonlinear contact conditions to evaluate five key factors: the effective range of forming fluid pressure, stress distribution within the component, plastic strain behavior, wall thickness variation, and protrusion height. The results revealed a common effective pressure range for both joint types. Compared to the T-joint, the X-joint exhibited less thinning at the protrusion apex and achieved a greater protrusion height. Overall, this study provides a reliable simulation framework for optimizing the THF process, reducing the experimental costs, and enhancing the quality of hollow joint production.

Keywords-tube hydroforming; copper hollow joints; finite element analysis; process optimization

I. INTRODUCTION

The THF process provides significant advantages over traditional metal forming methods, such as stamping, welding, and casting [1]. Its key benefits include the ability to create complex, integrated geometries, such as 3D profiles with variable cross-sections and hollow protrusions at different angles in a single operation. This eliminates the need for multi-piece stamping-welding assemblies, reduces the weld lines, enhances the structural integrity, and lowers the assembly costs. THF also enables weight reduction through optimal material distribution and thin walls, which is especially valuable in automotive and aerospace applications. Additionally, cold working during the process improves the mechanical properties by inducing work-hardening, thereby increasing the strength, stiffness, and fatigue resistance while ensuring a more uniform wall thickness. The process also produces smooth surfaces that minimize secondary machining, provides low springback for dimensional stability, reduces material waste compared to stamping, and offers lower tooling costs for medium production volumes [2-4]. However, THF also presents challenges. It requires a high initial investment, and not all materials are suitable. High-strength steels or thick-walled tubes, for example, may crack or wrinkle unless warm THF is used. Design constraints also exist, such as the requirement that the minimum corner radius be three to four times the material thickness, with a smaller radius demanding exponentially higher pressure.

Furthermore, the process is complex, requiring precise control of the internal fluid pressure, axial feeding, and lubrication [5, 6]. Research has extensively investigated the optimization of THF processes for T- and X-shaped joints. Authors in [7, 8] demonstrate the superiority of advanced modeling techniques, with the latter combining FEM and Artificial Neural Networks (ANN) to predict the optimal parameters accurately, reducing the thickness prediction error below 5% and cutting the experimental costs by 30%-40%. A critical focus across studies is managing the interfacial friction, identified in [9, 10] as a primary factor controlling the material flow, wall thickness distribution, and residual stresses. An optimal friction coefficient (μ) of 0.05-0.1 is proposed to balance formability and prevent failure. At the micro-scale, authors in [11] found SUS304 stainless steel more suitable than copper for micro T-joints due to its superior resistance to bending. Furthermore, comparative analyses of joint geometry reveal that X-joints, while requiring higher forming pressure, can offer a more uniform wall thickness distribution than T-joints, though they are more prone to extreme thinning. Collectively, these findings underscore that successful THF relies on the synergistic control of pressure paths, friction conditions, and material selection tailored to the specific joint geometry.

Numerical simulation based on the FEM is extensively applied in both research and industrial manufacturing for metal forming processes, owing to its significant advantages, such as reduced product design and development time, and the early prediction of potential defects or failures [12-14]. A 3D numerical simulation study of the THF process for forming a small protrusion on a T-shaped hollow joint from a seamless copper tube blank was conducted using Abaqus/CAE software

[15]. A comprehensive analysis and the comparison of key criteria were performed, including: the effective range of the forming fluid pressure (a key process parameter), the distribution of forming stress within the component, the components of PE in the part, the distribution of tube wall thickness, and the height of the small protrusion.

II. MATERIALS AND METHODS

A. *Geometric Model, Mesh Model, and Material Model of the Tubular Blank and Geometric Model of the Forming Die*

A tubular blank with an outer diameter of D_0 = 22.22 mm, wall thickness of t_0 = 1.2 mm, and length of l_0 = 120 mm was modeled. The geometric and mesh models were constructed for half of the tubular blank, as illustrated in Figures 1(a) and 1(b). The material model for the copper tubular blank, incorporating its material properties, is listed in Table I. The geometric model of the die assembly, comprising the lower die, left punch, and right punch, is presented in Figure 2. The key dimensions for both the T-shaped and X-shaped hollow joint forming dies include a length of 130 mm, a width of 110 mm, and a thickness of 25 mm [16]. The die cavity for housing the blank has a diameter equal to the blank's outer diameter (D_0). The die cavity for forming the small protrusion has a diameter of D_p = 19.05, which is less than D_0 ($D_p < D_0$ = 22.22 mm). The fillet radius in the transition region of the die is R_f = 5 mm, as depicted in Figure 2.

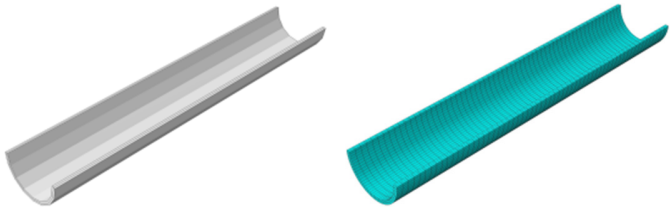

(a) (b)

Fig. 1. (a) Geometrical model of the tube blank and (b) its finite element mesh configuration.

TABLE I. MATERIAL PROPERTIES OF THE COPPER TUBE BLANK

Parameters	Value
Temperature (°C)	24
Density, ρ (kg/m^3)	8940
Young's modulus, E (Gpa)	115
Hardening coefficient, K (MPa)	325
Work hardening exponent, n	0.54
Poisson's ratio, v	0.33
Yield strength (MPa)	57.08
Ultimate tensile strength (MPa)	231.09
Elongation (%)	42.75

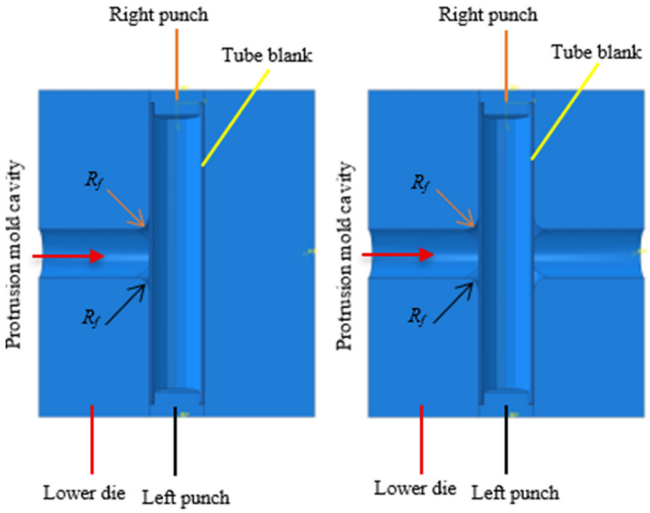

Fig. 2. Assembly module setup for numerical analysis of the THF process.

B. *Boundary Condition Setup for the Finite Element Analysis Simulation*

The THF process for forming T-shaped and X-shaped hollow joints was simulated using Abaqus/Explicit. In the model, the lower die half, left punch half, and right punch half were defined as discrete rigid bodies, while the half-tubular blank was treated as a deformable body with an elastic–plastic material definition. The blank was meshed with 2340 elements, using quadrilateral S4R elements generated through a free meshing technique with a medial axis algorithm. The contact interactions between surfaces were modeled with a penalty friction law, applying a friction coefficient of μ = 0.1 [1, 2].

The minimum internal fluid pressure (P_{min}) required to avoid wrinkling during the formation of the T and X-joints can be estimated using [1]:

$$P_{min} = \left(0.13 + 1.15\frac{t_0}{D_p}\right)\sigma_Y \quad (1)$$

The maximum pressure (P_b) that can be applied without causing fracture at the protrusion apex for the T and X hollow joints can be predicted by [17]:

$$P_b = \sigma_U\left(\frac{4t_0}{D_p - t_0}\right) \quad (2)$$

Given the parameter values for these equations: σ_Y = 57.08 MPa (yield strength), σ_U = 231.09 MPa (ultimate tensile strength), t_0 = 1.2 mm (initial wall thickness), and D_p = 19.05 mm (protrusion diameter), the calculated values are P_{min} = 7.96 MPa and P_b = 62.14 MPa. This pressure range provides an initial basis for determining the effective forming pressure window. The internal fluid pressure loading curve (Amp-1) and the axial feed loading curve for each tube end (Amp-2) were defined according to the 20-s forming cycle detailed in Table II. An identical set of boundary conditions was established for both forming simulations to enable a consistent comparative analysis of the formability of the T and X hollow joints.

TABLE II. LOADING CURVES OF THE FORMING PROCESS

Amp-1 loading path	
Time/frequency	Amplitude
0	0
0.5	1
1	1
Amp-2 loading path	
Time/frequency	Amplitude
0	0
0.5	0.5
1	1

Based on data concerning the axial feed provision, the forming fluid pressure range, and the numerical simulation outcomes of the two THF processes, in this study, a comprehensive analysis and comparison were conducted based on four specific criteria detailed in the subsequent section.

III. RESULTS AND DISCUSSION

A. *Effective Range of Forming Fluid Pressure*

Figure 3 indicates that the effective pressure range for forming the small protrusion in both T and X components is achieved with a maximum internal fluid pressure loading curve (Amp-1) of $P_{i\text{-}max}$ = 30 MPa-40 MPa, and an axial feed loading curve (Amp-2) of Af = 25 mm per tube end. Based on this effective forming pressure window, the four key output parameters of the forming process were studied and analyzed in greater depth.

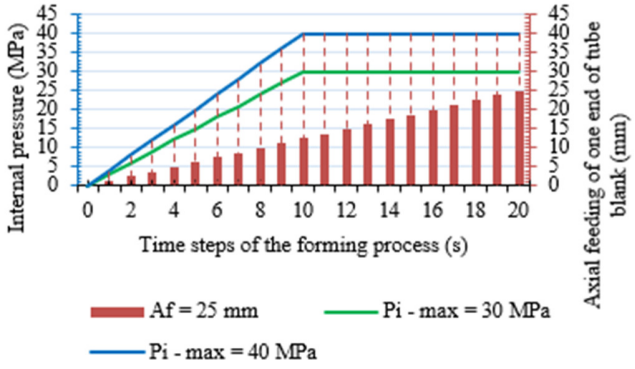

Fig. 3. Effective forming fluid pressure range for the small protrusion.

Increasing the $P_{i\text{-}max}$ value beyond this effective pressure range can lead to excessive thinning beyond the safe design limit (ε_{min} = -30%) and cause fracture at the small protrusion apex during formation due to excessive biaxial stretching. When the pressure was increased to $P_{i\text{-}max}$ = 45 MPa, for the T-shaped hollow component, thinning occurred at the protrusion apex ($t_{min\text{-}T}$ = 0.87 mm) at step 9, followed by fracture at step 10, as shown in Figure 4(a); for the X-shaped hollow component, thinning was observed at the protrusion apex ($t_{min\text{-}X}$ = 0.80 mm) at step 10, with fracture occurring at step 11, as portrayed in Figure 4(b).

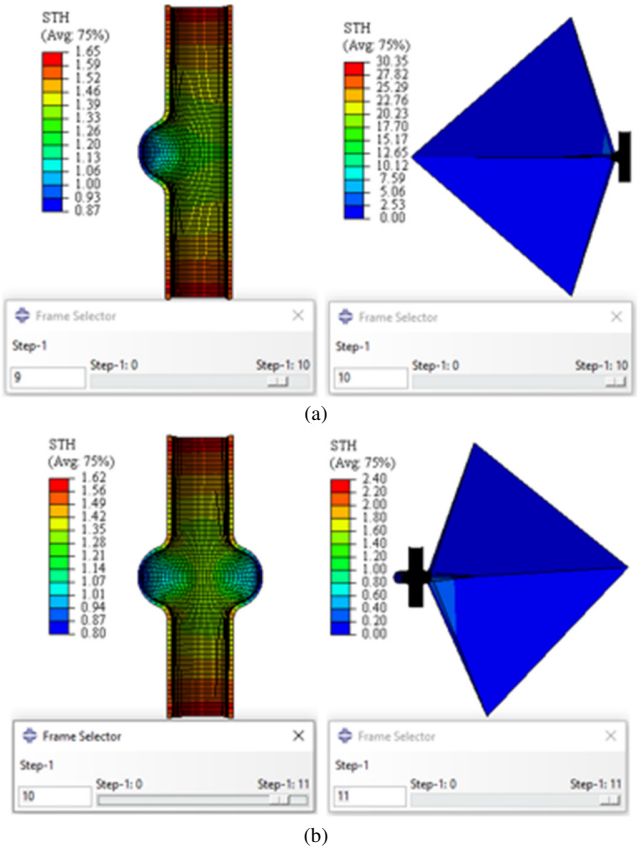

Fig. 4. Critical fluid pressure limit causing fracture at the small protrusion apex with process parameters $P_{i\text{-}max}$ = 45 MPa, Af = 25 mm: (a) T-joint, (b) X-joint.

B. *Distribution of Forming Stress within the Component*

The distribution of Von Mises forming stress in the two T and X hollow joints, with $P_{i\text{-}max}$ = 40 MPa and Af = 25 mm, is displayed in Figure 5. For the T-joint, the forming stress reached a maximum value of S_{max} = 231.09 MPa throughout the guiding zone (subject to axial compressive stress S33) and the transition zone (subject to high shear stress S12 due to bending and friction with the die wall). The stress distributed in the expansion zone, where the small protrusion is formed, remained within the safe limit of 69.63 MPa-231.09 MPa. Conversely, for the X-joint, the forming stress reached S_{max} = 231.09 MPa throughout the transition zone (due to high shear stress S12 from bending and die wall friction), while the stress in the guiding zone and the expansion zone (small protrusion formation) remained within the safe limit of 69.63 MPa-231.09 MPa. Reaching the maximum stress value in these zones is not harmful, since the tube wall is firmly pressed against the die cavity. This condition increases the component's stiffness and strength through work hardening, a key feature of the THF process. In the die cavity region where the protrusion forms, the tube wall undergoes plastic deformation driven by internal fluid pressure, which directs the material flow into the expansion zone to create the protrusion. At the protrusion apex, the material experiences a dominant biaxial stress state (S11, S22), posing a risk of fracture if the stress exceeds σU = 231.09 MPa. To ensure safety, the Von Mises stress at this location

should remain below 90% of σU. Although the forming stress reaches its maximum value, it remains within safe limits for the protrusion wall, which stays in continuous contact with the die profile.

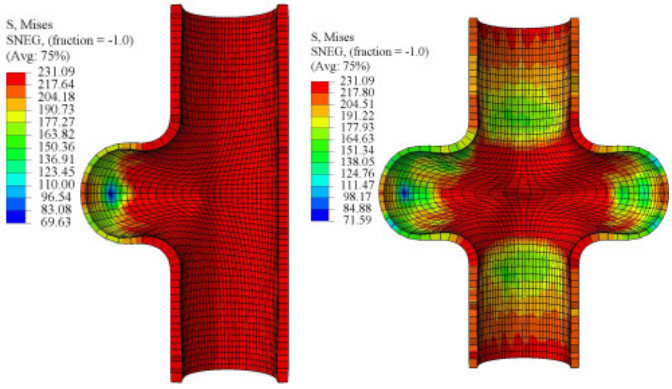

Fig. 5. Forming stress distribution in the component with process parameters P_{i-max} = 40 MPa, Af = 25 mm: (a) T-joint, (b) X-joint.

C. Plastic Strain Components in the Components

The PE components in the two T and X components formed with a fluid pressure of P_{i-max} = 40 MPa and Af = 25 mm are shown in Figures 6(a) and 6(b), respectively, illustrating the nonlinear plastic deformation behavior of the copper material. In the guiding zones at both tube ends of both components, the strain components exhibit negative values, PE_{min-T} = -0.15 and PE_{min-X} = -0.14, as depicted in Figure 6, due to the axial compressive stress (S33), which acts to feed material into the transition and expansion zones during formation. However, the hollow X-joint (featuring two small symmetrical protrusions) demonstrates a more balanced and symmetrical PE distribution compared to the hollow T-joint, which has only one small protrusion. The transition zone for small protrusion formation in both the T and X joints consists of two parts: material flow along the tube's axial direction and material flow perpendicular to the tube axis. For the T-joint, the axial material flow section exhibits negative strain components (PE_T = -0.15 to -0.07) due to compressive stress, while the section with material flow perpendicular to the tube axis shows positive strain components (PE_T = 0.01 to 0.82) due to tensile stress. The maximum value, PE_{max-T} = 0.82 (in the region experiencing high shear stress S12 from bending and die wall friction), is displayed in red on the scale and initiates from the center of the expanding blank, propagating towards the forming small protrusion. For the X-joint, the axial material flow section has negative strain components (PE_X = -0.14 to -0.02), and the perpendicular section shows positive strain components (PE_X = 0.11 to 1.36). The value PE_{max-X} = 1.36 is 1.66 times greater than PE_{max-T}, yet it still ensures safe formability for this region, as the tube wall remains in continuous contact with the die wall. The expansion zone of both components, dominated by a biaxial stress state (S11, S22), exhibits positive PE values ranging from 0.09 to 0.74, ensuring the safe formability of the small protrusion.

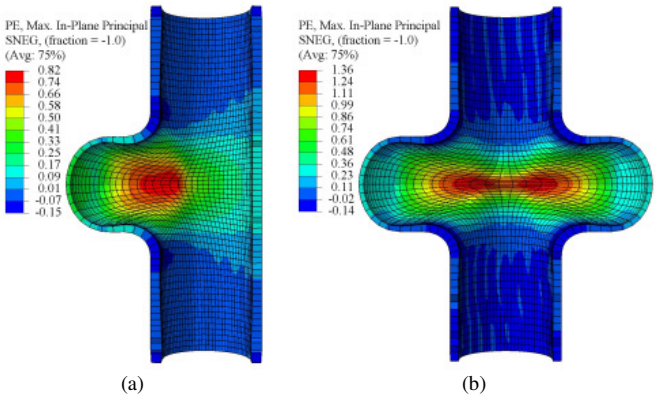

Fig. 6. PE component distribution in the component with process parameters P_{i-max} = 40 MPa, Af = 25 mm: (a) T-joint, (b) X-joint.

The values of PE_{max} in both components across the effective forming pressure range are presented in the chart in Figure 7. The chart shows that their PE_{max} values increase with rising internal fluid pressure. At a fluid pressure of P_{i-max} = 30 MPa, $PE_{max-T\ (30MPa)}$ = 0.77 is less than $PE_{max-X\ (30MPa)}$ = 1.29, indicating a significant difference of $\Delta PE_{max\ (30MPa)} = PE_{max-X\ (30MPa)} - PE_{max-T\ (30MPa)}$ = 0.52 during small protrusion formation. Similarly, at P_{i-max} = 35 MPa, $PE_{max-T\ (35MPa)} = 0.80 < PE_{max-X\ (35MPa)}$ = 1.33, with $\Delta PE_{max\ (35MPa)}$ = 0.53; and at P_{i-max} = 40 MPa, $PE_{max-T\ (40MPa)} = 0.82 < PE_{max-X\ (40MPa)}$ = 1.36, with $\Delta PE_{max\ (40MPa)}$ = 0.54. This also demonstrates that the difference in ΔPE_{max} between the T and X components gradually increases with higher internal fluid pressure.

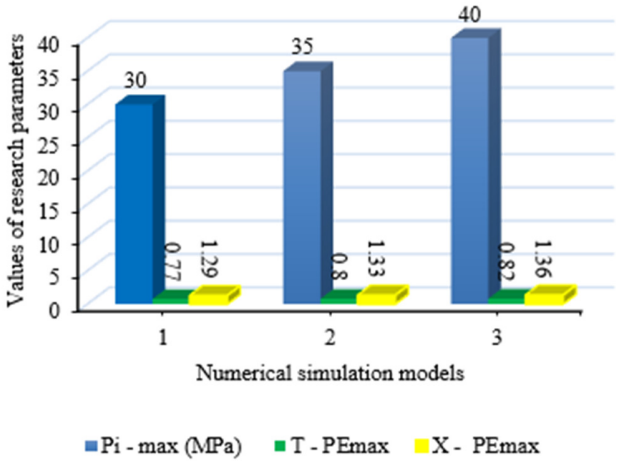

Fig. 7. Comparison of PE components in the component across the effective forming fluid pressure range for the small protrusion.

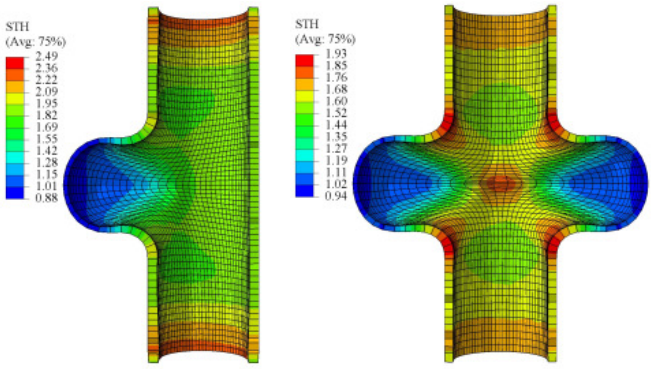

(a) (b)

Fig. 8. Wall thickness distribution in the component with process parameters P_{i-max} = 40 MPa, Af = 25 mm: (a) T-joint, (b) X-joint.

The wall thickness (STH) distribution in the two T and X hollow joints, formed with P_{i-max} = 40 MPa and Af = 25 mm, is illustrated in Figure 8. The STH within each joint is non-uniform across the guiding zone, transition zone, and the expansion zone where the small protrusion is formed, due to the different stress-strain states experienced during the forming process. Wall thickening occurs in both the guiding and transition zones of both components. At the tube ends of the T-joint, the maximum thickness reaches STH_{max-T} = 2.49 mm (a thickening ratio of 107%). At the four filleted corners of the transition zone in the X-joint, the maximum thickness is STH_{max-X} = 1.93 mm (a thickening of 60.83%). The STH in the guiding zone of the X-joint is distributed more uniformly, ranging from 1.6 mm to 1.76 mm, compared to the T-joint, which ranges from 1.82 mm to 2.49 mm. The STH in the transition zone of both components is quite similar along the tube's axial direction, ranging from 1.55 mm to 1.93 mm. Perpendicular to the tube axis, the STH distribution in the transition zone is also comparable for both joints, ranging from 1.2 mm to 1.82 mm. Wall thinning primarily occurs at the spherical crown section of the small protrusion in both components. For the T-joint, the minimum thickness is STH_{min-T} = 0.88 mm (a thinning ratio of ε_{min-T} = -26.67%), as shown in Figure 8(a). For the X-joint, the minimum thickness is STH_{min-X} = 0.94 mm (a thinning ratio of ε_{min-X} = -21.67%), as portrayed in Figure 8(b). The thinning ratios for both components meet the required criteria, as they are greater than the allowable limit for copper hollow joints of ε_{min} = -30% (corresponding to STH_{min} = 0.84 mm). The STH_{min} values for both joints across the effective forming pressure range are compared with each other and with the initial blank thickness (t_0) in the chart in Figure 9. It is observed that increasing the P_{i-max} pressure value reduces the STH_{min}, yet it remains greater than STH_{min} = 0.84 mm. The reduction in wall thickness is more pronounced at the spherical crown of the small protrusion in the T-joint: t_0 = 1.2 mm → 1.01 mm (P_{i-max} = 30 MPa) → 0.95 mm (P_{i-max} = 35 MPa) → 0.88 mm (P_{i-max} = 40 MPa), compared to the X-joint: t_0 = 1.2 mm → 1.06 mm (P_{i-max} x = 30 MPa) → 1.00 mm (P_{i-max} = 35 MPa) → 0.94 mm (P_{i-max} = 40 MPa).

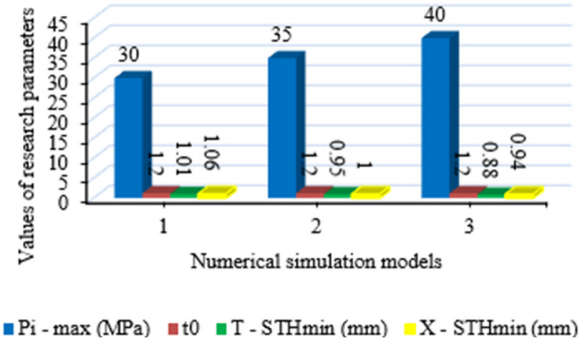

Fig. 9. Comparison of STH_{min} in the component across the effective forming fluid pressure range for the small protrusion.

D. Height of the Small Hollow Protrusion

The height of the small protrusion (U1) in the two T and X hollow joints, formed with P_{i-max} = 40 MPa and Af = 25 mm, is displayed in Figure 10. For the T-joint, the height is $U1_T$ = |-17.10| mm, as depicted in Figure 10(a). For the X-joint, the height of a single small protrusion is $U1_X$ = |-18.40| mm, and the combined height of both protrusions is $2U1_X$ = 36.80 mm (Figure 10(b)). The ratio of the protrusion height to the initial tube outer diameter (D_0 = 22.22 mm) for the T-joint is $U1_T$ / D_0 = 17.10 / 22.22 = 0.77. This is less than the ratio for a single protrusion in the X-joint, which is $U1_X$ / D_0 = 18.40 / 22.22 = 0.83, and significantly less than the ratio for both protrusions, $2U1_X$ / D_0 = 36.80 / 22.22 = 1.66. This indicates that the effective protrusion height achieved in the X-joint is greater than that in the T-joint. The protrusion height (U1) for both joints across the effective forming pressure range, with a total axial feed of Af_Σ = 50 mm, is compared in the chart in Figure 11. It is observed that increasing the P_{i-max} pressure value increases the small protrusion height. For the T-joint: $U1_{T(30MPa)}$ = 15.01 mm → $U1_{T(35MPa)}$ = 16.01 mm → $U1_{T(40MPa)}$ = 17.10 mm. For the X-joint: $U1_{X(30MPa)}$ = 16.13 mm → $U1_{X(35MPa)}$ = 17.25 mm → $U1_{X(40MPa)}$ = 18.40 mm, resulting in a combined height of $2U1_{X(30MPa)}$ = 32.26 mm → $2U1_{X(35MPa)}$ = 34.50 mm → $2U1_{X(40MPa)}$ = 36.80 mm. The results demonstrate that the formation of the total height of the two small protrusions (2U1) in the X-joint is more efficient relative to the total axial feed (Af_Σ) compared to the formation of the single protrusion height (U1) in the T-joint.

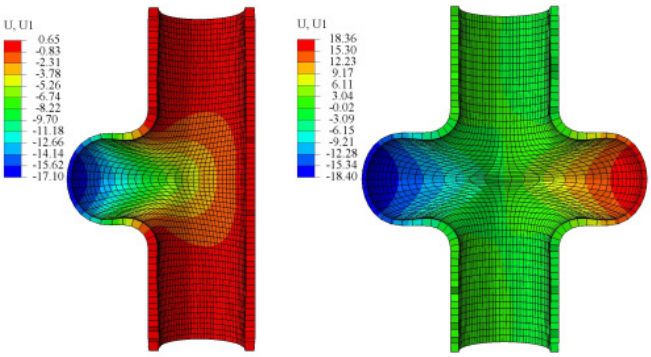

(a) (b)

Fig. 10. Height of the small protrusion in the component with process parameters P_{i-max} = 40 MPa, Af = 25 mm: (a) T-joint, (b) X-joint.

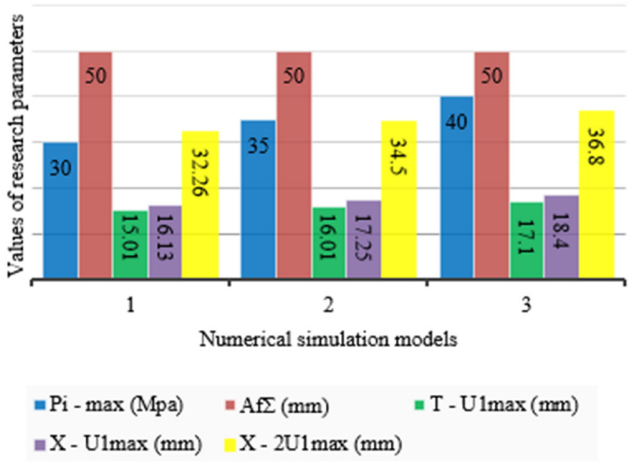

Fig. 11. Comparison of $U1_{max}$ in the component across the effective forming fluid pressure range for the small protrusion.

IV. CONCLUSIONS

This study provides a comprehensive numerical investigation of the Tube Hydroforming (THF) process for forming small protrusions (D_p / D_0 = 19.05 / 22.22) in copper T- and X-shaped hollow joints through Finite Element Method (FEM) in Abaqus/Explicit. The key findings, novel contributions, and limitations are summarized as follows:

- Both joint configurations achieved successful formation within an optimal forming fluid pressure range of $P_{i–max}$ = 30 MPa-40 MPa and axial feed of Af = 25 mm per tube end. The T-joint exhibited a PE_{max-T} of 0.82 with wall thinning of 26.67% (STH_{min-T} = 0.88 mm) and a final protrusion height of 17.10 mm. The X-joint demonstrated superior performance with PE_{max-X} = 1.36, a reduced wall thinning of 21.67% (STH_{min-X} = 0.94 mm), and significantly greater total protrusion height ($2U1_{max-X}$ = 36.80 mm).
- The present study establishes the first comparative framework for THF process optimization between T- and X-shaped copper joints, and identifies distinct forming characteristics: the X-joints provide better material distribution and higher formability despite higher strain concentrations. It also develops predictive models for key output parameters (wall thinning, protrusion height) based on input process variables.
- The study focuses specifically on copper material properties; future research should investigate other ductile materials and elevated temperature forming. Experimental validation is required to confirm the numerical predictions and refine the friction models. Further investigation should explore the multi-objective optimization considering energy consumption and cycle time reduction. The research can be extended to include more complex joint geometries and scaled-up industrial applications

This work provides a foundational framework for optimizing the THF processes in hollow joint manufacturing, offering practical guidelines for die design and process parameter selection that balance the formability constraints with the structural performance requirements.

REFERENCES

[1] M. Koç, *Hydroforming for Advanced Manufacturing*. Elsevier, 2008.

[2] N. V. Pham, Hydraulic Stamping Technology. Hanoi University of Science and Technology, 2006.

[3] P. V. Reddy, B. V. Reddy, and P. J. Ramulu, "Evolution of Hydroforming Technologies and Its Applications — A Review," *Journal of Advanced Manufacturing Systems*, vol. 19, no. 04, pp. 737–780, Dec. 2020, https://doi.org/10.1142/S0219686720500341.

[4] C. Bell, J. Corney, N. Zuelli, and D. Savings, "A state of the art review of hydroforming technology," *International Journal of Material Forming*, vol. 13, no. 5, pp. 789–828, Sept. 2020, https://doi.org/10.1007/s12289-019-01507-1.

[5] Schuler, *Metal Forming Handbook*. Springer Science & Business Media, 1998.

[6] C. V. Nielsen and P. A. F. Martins, *Metal Forming: Formability, Simulation, and Tool Design*. Academic Press, 2021.

[7] P. Ray and B. J. Mac Donald, "Experimental study and finite element analysis of simple X- and T-branch tube hydroforming processes," *International Journal of Mechanical Sciences*, vol. 47, no. 10, pp. 1498–1518, Oct. 2005, https://doi.org/10.1016/j.ijmecsci.2005.06.007.

[8] F. Abbassi, F. Ahmad, S. Gulzar, T. Belhadj, A. Karrech, and H. S. Choi, "Design of T-shaped tube hydroforming using finite element and artificial neural network modeling," *Journal of Mechanical Science and Technology*, vol. 34, no. 3, pp. 1129–1138, Mar. 2020, https://doi.org/10.1007/s12206-020-0214-4.

[9] A. Fiorentino, E. Ceretti, A. Aldo, D. Braga, and C. Giardini, "Experimental Study of Lubrication Influence in the Production of Hydroformed T-Joint Tubes," *Key Engineering Materials*, vol. 410–411, pp. 15–24, 2009, https://doi.org/10.4028/www.scientific.net/KEM.410-411.15.

[10] A. Ktari, A. Abdelkefi, N. Guermazi, P. Malecot, and N. Boudeau, "Numerical investigation of plastic flow and residual stresses generated in hydroformed tubes," *Proceedings of the Institution of Mechanical Engineers, Part L: Journal of Materials: Design and Applications*, vol. 235, no. 5, pp. 1100–1111, May 2021, https://doi.org/10.1177/1464420721989746.

[11] H. Yasui, S. Yoshihara, S. Mori, K. Tada, and K. Manabe, "Material Deformation Behavior in T-Shape Hydroforming of Metal Microtubes," *Metals*, vol. 10, no. 2, Feb. 2020, Art. no. 199, https://doi.org/10.3390/met10020199.

[12] M. T. Trinh, D. T. Nguyen, T. Q. Pham, A. N. Pham, and V. D. Dinh, "Hydro-Forming a Cross-Shaped Component from Tube Billet," *Journal of Machine Engineering*, vol. 25, no. 2, pp. 111–122, May 2025, https://doi.org/10.36897/jme/204661.

[13] M. T. Trinh, T. D. Nguyen, Q. T. Pham, A. N. Pham, and D. V. Dinh, "Hydro-Forming of U-Shaped Parts with Branches," *Engineering, Technology & Applied Science Research*, vol. 15, no. 1, pp. 19226–19231, Feb. 2025, https://doi.org/10.48084/etasr.9227.

[14] V. D. Quang, "The Optimization of Rotary Bending Die Process: Criteria for the Metal Sheet Angles and Springback Effects," *Engineering, Technology & Applied Science Research*, vol. 15, no. 1, pp. 20553–20558, Feb. 2025, https://doi.org/10.48084/etasr.9706.

[15] "Explicit," *Dassault Systèmes*, Aug. 25, 2023. https://www.3ds.com/products/simulia/abaqus/explicit.

[16] R. Neugebauer, Ed., *Hydro-Umformung*. Berlin, Heidelberg: Springer Berlin Heidelberg, 2007.

[17] S. Jirathearanat, C. Hartl, and T. Altan, "Hydroforming of Y-shapes—product and process design using FEA simulation and experiments," *Journal of Materials Processing Technology*, vol. 146, no. 1, pp. 124–129, Feb. 2004, https://doi.org/10.1016/S0924-0136(03)00852-5.